ISSN 1330-3651 (Print), ISSN 1848-6339 (Online) https://doi.org/10.17559/TV-20220115101756
Preliminary communication

Ultrasonic Detection of Residual Stress Field of Barrel Inner Wall

Wentao SONG, Zengxu ZHAO*

Abstract: Residual stress has a significant impact on the service performance of mechanical components, especially in terms of strength, fatigue life, and dimensional stability. It has long been a key difficulty to evaluate the residual stress state on the surface or at a certain depth of members in a rapid, nondestructive, and accurate manner. To address the problem, this paper explores the correlations of ultrasonic speed and direction with stress, and compares the sensitivity of different ultrasounds to stress, with the help of acoustic elasticity theory and ultrasonic nondestructive detection technology. The comparison shows the speed of the longitudinal wave propagating along the stress direction suffers the greatest influence from stress. Next, a residual stress ultrasound detection system was constructed: a critically refracted longitudinal wave (L_{CR} wave) was excited by pitch-catch oblique incidence within a certain depth of the measured material, and the residual stress was derived from the variation of propagation time in a fixed propagation distance. On this basis, a curved acoustic wedge was designed for tubular members. Considering the stability of the coupling layer and the bottom echo, a precise propagation time measurement algorithm was proposed. Finally, ultrasound detection was carried out excellently on the self-compacting stress field of the inner wall of in-service tubular members. The research lays the foundation for applying the ultrasonic method to stress field detection of similar members.

Keywords: barrel inner wall; nondestructive testing; residual stress field; surface member; ultrasound

1 INTRODUCTION

Residual stress is the inherent stress of members that maintain the internal balance, in the absence of external factors. Residual stress is inevitable in mechanical machining (e.g., squeezing, drawing, rolling, correction, cutting, grinding, surface rolling, shot blasting, and hammering) and hot working (e.g., welding, and cutting). Normally, residual stress has a harmful effect. For example, residual stress, coupled with working temperature, and working medium, causes a substantial decline of members in the resistance to fatigue, brittle breaking, and stress corrosion cracking, and dimensional stability [1]. In addition, the accumulation of residual stress on member surface is likely to have the risks caused cracks on or near the surface. Therefore, it is very meaningful to develop an effective way to detect residual stress, and evaluate the service state of members.

Residual stress detection technique can be traced back to the 1930s. So far, dozens of detection methods have been developed. By their damages to the members, these methods can be divided into destructive techniques, semi-destructive techniques, and nondestructive techniques. The destructive techniques include slice method, contour method, etc. [2]. The semi-destructive techniques include blind hole method, ring core method, and deep hole method. Both destructive and semi-destructive techniques release stress during the application. Typical nondestructive techniques are X-ray diffractometry (XRD), neutron diffractometry, magnetic assay, scanning electron acoustic microscopy (SEAM), and ultrasonic method [3]. By comparing the various detection methods, it regarded the ultrasonic method as the most quick and convenient technique for nondestructive detection of residual stress of barrel inner wall, for its high resolution, high permeability, and no damage to the human body.

Ultrasonic stress detection is based on the linear relationship between ultrasound speed and material stress. This relationship is the acoustic elasticity effect exhibited within the elastic limit of the material. Drawing on the acoustic elasticity theory, this paper explores the correlations of ultrasonic speed and direction with stress, compares the sensitivity of different ultrasounds to stress, and analyzes the generation principle of critically refracted longitudinal wave (L_{CR} wave). On this basis, scientific issues on the law of stress and wave propagation were solved, and a precise propagation time measurement algorithm was improved. Finally, the proposed ultrasonic detection system was applied to detect the self-compacting stress of the inner wall of in-service tubular members, and plot the distribution of the residual stress field.

2 ACOUSTIC ELASTICITY THEORY

Based on the mechanics of finitely deformed continuous medium, the acoustic elasticity theory studies the relationship between the stress state of elastic solid and the speed of elastic wave from the macroscopic perspective. It is one of the main bases for ultrasonic determination of stress.

There are four basic assumptions of the theory: (1) The solid is super elastic and uniform; (2) The solid is a continuous medium (because the elastic wave length is much greater than the grain size and micro defects of the solid); (3) The small disturbances of the acoustic wave are superimposed into the finite static deformation of the solid; (4) The solid deformation is an isothermal or isentropic process. When the solid is in a state of zero stress and zero strain, it is called the initial state. The initial coordinate system is established (Fig. 1). The starting point of the particle position vector is the origin of Cartesian coordinates, and the three axes respectively represent the components of the particle position vector in this direction.

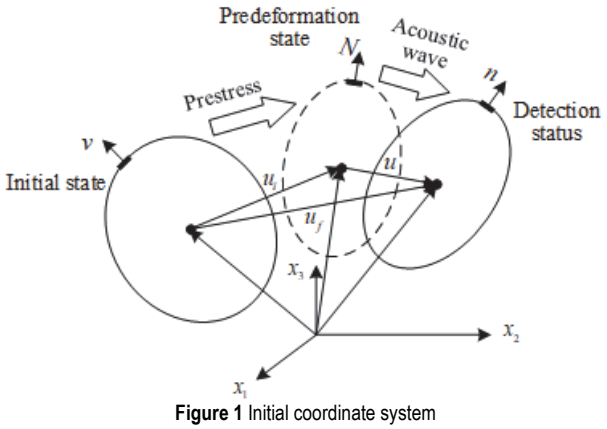

Figure 1 Initial coordinate system

Under the above assumptions, the elastic wave fluctuation equation (acoustic elasticity equation) in the stress medium under the initial coordinate system can be established [4]:

$$\frac{\partial}{\partial X_J}\left[\left(\delta_{IK}t^i_{JL}+C_{IJKL}\right)\frac{\partial u_K}{\partial X_L}\right]=\rho^i\frac{\partial^2 u_I}{\partial t^2} \tag{1}$$

where, δ_{IK} is the Kronecker Delta function; ρ^i is the solid density under stress; u_I is the dynamic displacement; X_J is the position vector of the particle; C_{IJKL} is the equivalent stiffness depending on the material constant and the initial displacement field; t^i_{JL} is the Cauchy stress of the solid under stress described with the initial coordinates.

As shown in Eq. (1), the acoustic elasticity equation is very complex and nonlinear. It can be simplified into a linear formula. Suppose the ultrasonic wave is planar wave, the wave can be described with the initial coordinates as [5]:

$$u_I=U_I\exp\left[ik\left(N_JX_J-Vt\right)\right] \tag{2}$$

where, k is the wave number ($k = 2\pi$/wave length); N is the unit normal direction of the planar wave, i.e., the cosine of the propagation direction; U is the amplitude.

For uniform deformation, the acoustic elasticity Eq. (1) of the initial coordinates can be simplified as:

$$\left(C_{IJKL}+\delta_{IK}t^i_{JL}\right)\frac{\partial u_K}{\partial X_J\partial X_L}=\rho^i\frac{\partial^2 u_I}{\partial t^2} \tag{3}$$

Substituting Eq. (2) into Eq. (3):

$$\left[C_{IJKL}N_JN_L+\left(t^i_{JL}N_JN_L-\rho^iV^2\right)\delta_{IK}\right]U_K=0 \tag{4}$$

The characteristic equation can be expressed as:

$$\left|D_{IK}-\rho^iV^2\delta_{IK}\right|=0 \tag{5}$$

where, the acoustic tensor can be expressed as:

$$D_{IK}=C_{IJKL}N_JN_L+\delta_{IK}t^i_{JL} \tag{6}$$

3 ULTRASONIC DETECTION THEORY OF RESIDUAL STRESS

3.1 Relationship Between Ultrasound and Stress

When the solid is isotropic, Eq. (4) can be parsed (the detailed process is shown in Pao, Y. H. and Sachse, W. work [6]). Hence, the speed of ultrasound in the solid as a function of stress can be established in the Cartesian coordinate system [7, 8]:

(1) Longitudinal wave propagating in the stress direction (Fig. 2a)

$$\rho_0V_{111}^2=\lambda+2\mu+\\+\frac{\sigma}{3\lambda+2\mu}\left[\frac{\lambda+\mu}{\mu}\left(4\lambda+10\mu+4m\right)+\lambda+2l\right] \tag{7}$$

(2) Longitudinal wave propagating perpendicular to the stress direction (Fig. 2b)

$$\rho_0V_{113}^2=\lambda+2\mu+\frac{\sigma}{3\lambda+2\mu}\left[2l-\frac{2\lambda}{\mu}\left(\lambda+2\mu+m\right)\right] \tag{8}$$

(3) Shear wave propagating along the stress direction, and polarizing perpendicular to the stress direction (Fig. 2c)

$$\rho_0V_{131}^2=\mu+\frac{\sigma}{3\lambda+2\mu}\left[\frac{\lambda n}{4\mu}+4\lambda+4\mu+m\right] \tag{9}$$

(4) Shear wave propagating and polarizing perpendicular to the stress direction (Fig. 2d)

$$\rho_0V_{132}^2=\mu+\frac{\sigma}{3\lambda+2\mu}\left[m-\frac{\lambda+\mu}{2\mu}n-2\lambda\right] \tag{10}$$

(5) Shear wave propagating perpendicular to the stress direction, and polarizing along the stress direction (Fig. 2e)

$$\rho_0V_{133}^2=\mu+\frac{\sigma}{3\lambda+2\mu}\left[\frac{\lambda n}{4\mu}+\lambda+2\mu+m\right] \tag{11}$$

(6) Surface wave propagating along the stress direction (Fig. 2f)

$$\left[\lambda+\alpha_{11}\alpha_{21}(\lambda+2\mu)\right]\left[1-\frac{(2\lambda+\mu)\sigma}{(3\lambda+2\mu)\mu}\right]+\lambda(1+\frac{\sigma}{\mu})=0 \tag{12}$$

where, $\alpha_{11}=\sqrt{1-(V_{11}/V_{1L})^2}$; $\alpha_{21}=\sqrt{1-(V_{11}/V_{1S})^2}$; V_{1L} and V_{1S} are the speeds of the longitudinal wave and shear wave in stress-free solid, respectively.

(7) Surface wave propagating perpendicular to the stress direction (Fig. 2g)

$$\left[\lambda+\alpha_{12}\alpha_{22}(\lambda+2\mu)\right]\left[1-\frac{(2\lambda+\mu)\sigma}{(3\lambda+2\mu)\mu}\right]+\lambda(1+\frac{\sigma}{\mu})=0 \tag{13}$$

where, $\alpha_{12}=\sqrt{1-(V_{12}/V_{1L})^2}$; $\alpha_{22}=\sqrt{1-(V_{12}/V_{1S})^2}$.

In Eqs. (7) to (13), λ and μ are the second-order elastic constants of the solid; l, m, and n are the third-order elastic constants of the solid; ρ_0 is the density of the solid before deformation; σ is the one-way stress applied on the solid (tensile stress is positive, and compressive stress is negative).

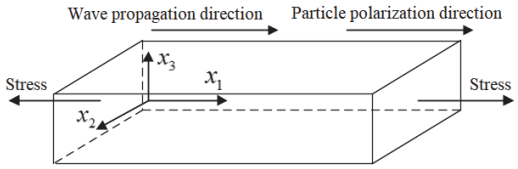

(a) Longitudinal wave propagating along the stress direction

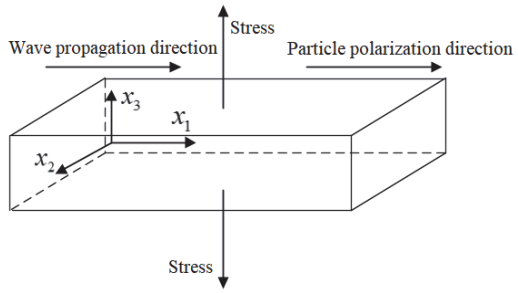

(b) Longitudinal wave propagating perpendicular to the stress direction

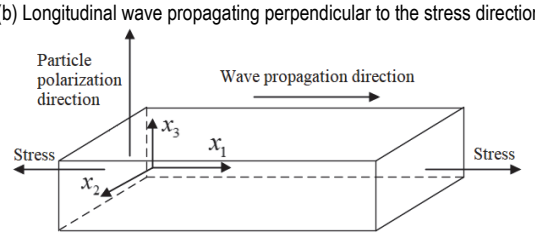

(c) Shear wave propagating along the stress direction, and polarizing perpendicular to the stress direction

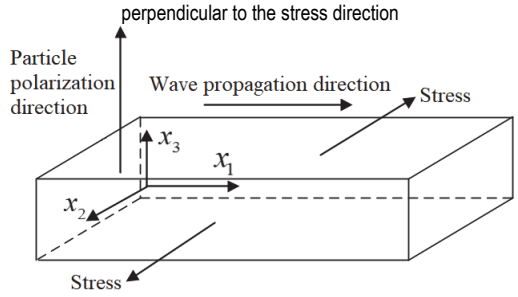

(d) Shear wave propagating and polarizing perpendicular to the stress direction

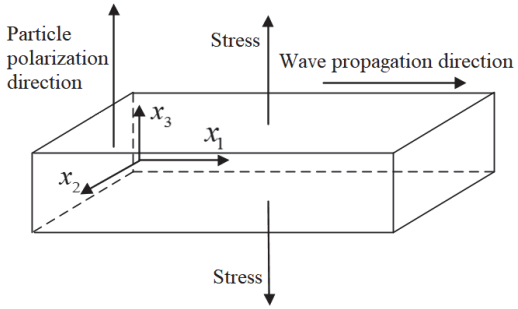

(e) Shear wave propagating perpendicular to the stress direction, and polarizing along the stress direction

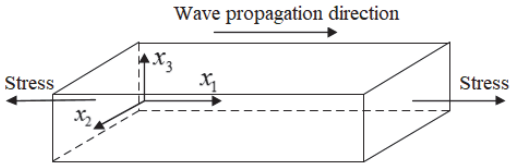

(f) Surface wave propagating along the stress direction

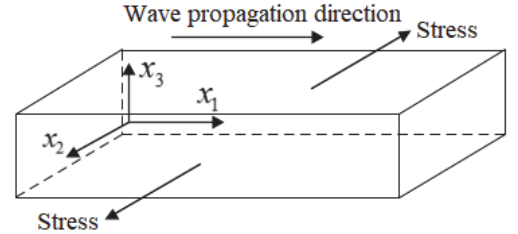

(g) Surface wave propagating perpendicular to the stress direction

Figure 2 Relationship between ultrasound and wave in Cartesian coordinate system

Note: For longitudinal and shear waves, the wave speed is described with three subscripts, e.g., V_{ABC}. The first subscript, second subscript, and third subscript represent the wave propagation direction, particle polarization direction, and one-way stress direction, respectively; for the surface wave, the wave speed is described with two subscripts, e.g., V_{AB}. The first subscript and second subscript represent the wave propagation direction, and one-way stress direction, respectively.

3.2 Sensitivity Comparison

Different types of ultrasonic waves vary in the sensitivity to stress. Finding the derivative of speed V to stress σ in Eqs. (7) to (13), we have $\mathrm{d}V = K_\alpha \mathrm{d}\sigma$, where K_α is the stress sensitivity coefficient. The greater the absolute value of K_α, the more sensitive the corresponding type of ultrasonic wave is to stress.

The derivation results of Eqs. (7) to (13) are as follows:

$$\mathrm{d}V_{111} = \frac{\left[\frac{\lambda+\mu}{\mu}(4\lambda+10\mu+4m)+\lambda+2l\right]}{2\rho_0 V_{111}(3\lambda+2\mu)}\mathrm{d}\sigma \tag{14}$$

$$\mathrm{d}V_{113} = \frac{\left[2l-\frac{2\lambda}{\mu}(\lambda+2\mu+m)\right]}{2\rho_0 V_{113}(3\lambda+2\mu)}\mathrm{d}\sigma \tag{15}$$

$$\mathrm{d}V_{131} = \frac{\left[\frac{\lambda n}{4\mu}+4\lambda+4\mu+m\right]}{2\rho_0 V_{131}(3\lambda+2\mu)}\mathrm{d}\sigma \tag{16}$$

$$\mathrm{d}V_{132} = \frac{\left[m-\frac{\lambda+\mu}{2\mu}n-2\lambda\right]}{2\rho_0 V_{132}(3\lambda+2\mu)}\mathrm{d}\sigma \tag{17}$$

$$\mathrm{d}V_{133} = \frac{\left[\frac{\lambda n}{4\mu}+\lambda+2\mu+m\right]}{2\rho_0 V_{133}(3\lambda+2\mu)}\mathrm{d}\sigma \tag{18}$$

$$\begin{cases} \mathrm{d}V_{11} = \dfrac{K_4}{K_1(K_2+K_3)}\mathrm{d}\sigma \\ K_1 = (\lambda+2\mu)\left[1-K_5\sigma\right] \\ K_2 = \dfrac{1}{2}\left(1-\dfrac{V_{11}^2}{V_{1L}^2}\right)^{-\frac{1}{2}}\left(-\dfrac{2V_{11}}{V_{1L}^2}\right)\left(1-\dfrac{V_{11}^2}{V_{1S}^2}\right)^{\frac{1}{2}} \\ K_3 = \dfrac{1}{2}\left(1-\dfrac{V_{11}^2}{V_{1L}^2}\right)^{\frac{1}{2}}\left(-\dfrac{2V_{11}}{V_{1S}^2}\right)\left(1-\dfrac{V_{11}^2}{V_{1S}^2}\right)^{-\frac{1}{2}} \\ K_4 = K_5K_6 - \dfrac{\lambda}{\mu} \\ K_5 = \dfrac{(2\lambda+\mu)}{(3\lambda+2\mu)\mu} \\ K_6 = \lambda+(\lambda+2\mu)\left(1-\dfrac{V_{11}^2}{V_{1L}^2}\right)^{\frac{1}{2}}\left(1-\dfrac{V_{11}^2}{V_{1S}^2}\right)^{\frac{1}{2}} \end{cases} \tag{19}$$

$$\begin{cases} \mathrm{d}V_{12} = \dfrac{K_4^{'}}{K_1^{'}\left(K_2^{'}+K_3^{'}\right)}\mathrm{d}\sigma \\ K_1^{'} = (\lambda+2\mu)\left[1-K_5^{'}\sigma\right] \\ K_2^{'} = \dfrac{1}{2}\left(1-\dfrac{V_{12}^2}{V_{1L}^2}\right)^{-\frac{1}{2}}\left(-\dfrac{2V_{12}}{V_{1L}^2}\right)\left(1-\dfrac{V_{12}^2}{V_{1S}^2}\right)^{\frac{1}{2}} \\ K_3^{'} = \dfrac{1}{2}\left(1-\dfrac{V_{12}^2}{V_{1L}^2}\right)^{\frac{1}{2}}\left(-\dfrac{2V_{12}}{V_{1S}^2}\right)\left(1-\dfrac{V_{12}^2}{V_{1S}^2}\right)^{-\frac{1}{2}} \\ K_4^{'} = K_5^{'}K_6^{'}-\dfrac{\lambda}{\mu} \\ K_5^{'} = \dfrac{(2\lambda+\mu)}{(3\lambda+2\mu)\mu} \\ K_6^{'} = \lambda+(\lambda+2\mu)\left(1-\dfrac{V_{12}^2}{V_{1L}^2}\right)^{\frac{1}{2}}\left(1-\dfrac{V_{12}^2}{V_{1S}^2}\right)^{\frac{1}{2}} \end{cases} \quad (20)$$

Tab. 1 lists the elastic constants of different solid materials [9].

Table 1 Second- and third-order constants of materials / GPa

Material	λ	μ	l	m	n
Steel (0.12% C)	115	82	–301 ± 37	–666 ± 6.5	–716 ± 4.5
Aluminum (99%)	61 ± 1	25	–47 ± 25	–342 ± 10	–248 ± 10
Copper (99.9%)	104	46	–542 ± 30	–372 ± 5	–401 ± 5

To examine the sensitivity of different types of ultrasonic waves to steel stress, the elastic constants of steel were substituted into Eqs. (14) to (20), with the steel density of 7.85 g/cm^3. Considering the limited variation of stress with sound speeds, the speeds under zero stress state $V_{111} = V_{113} = 5.90$ km/s, and $V_{131} = V_{132} = V_{133} = 3.20$ km/s, were substituted into Eqs. (14) to (18):

For Eq. (14): $\mathrm{d}V_{111} \approx -0.08085\mathrm{d}\sigma$;
For Eq. (15): $\mathrm{d}V_{113} \approx 0.01025\mathrm{d}\sigma$;
For Eq. (16): $\mathrm{d}V_{131} \approx -0.00505\mathrm{d}\sigma$;
For Eq. (17): $dV_{132} \approx -0.00505d\sigma$;
For Eq. (18): $\mathrm{d}V_{133} \approx -0.02495\mathrm{d}\sigma$.

As shown in Eqs. (19) and (20), the sensitivity of surface wave to stress has a complex nonlinear relationship with the transverse and horizontal wave speeds in the solid material under stress, as well as the stress of the surface wave, and the stress magnitude. Substituting stress $\sigma = 100$ MPa, $V_{11} = 3.0$ km/s, $V_{1L} = 5.9$ km/s, and $V_{1S} = 3.2$ km/s into Eqs. (19) and (20), we have:

$$\mathrm{d}V_{11} \approx dV_{12} \approx -0.00153\mathrm{d}\sigma$$

Fig. 3 compares the influence of stress on the speed of various types of ultrasonic waves propagating in steel. By the sensitivity to stress, the different types of ultrasonic waves can be ranked in descend order as longitudinal wave propagating in the stress direction > shear wave propagating perpendicular to the stress direction, and polarizing along the stress direction > longitudinal wave propagating perpendicular to the stress direction > shear wave propagating along the stress direction, and polarizing perpendicular to the stress direction = shear wave propagating and polarizing perpendicular to the stress direction > surface wave propagating along the stress direction = surface wave propagating perpendicular to the stress direction.

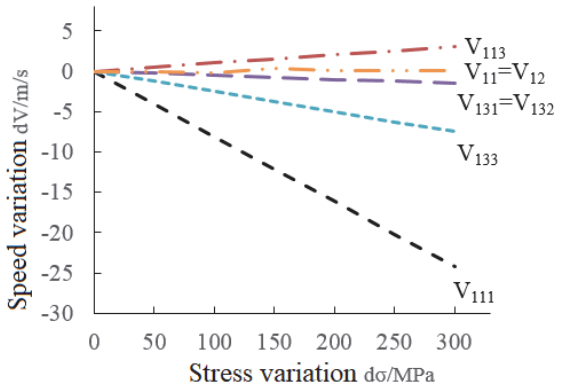

Figure 3 Influence of stress on the speed of various types of ultrasonic waves

3.3 L_{CR} Wave Method

According to Snell's law, when a longitudinal wave propagates from a medium with a slow sound speed to a medium with a fast sound speed, there will be an incident angle making the refractive angle of the refractive longitudinal wave equal to 90°. The longitudinal wave of the refractive angle of 90° is a critically refracted longitudinal wave (L_{CR}), while the incident angle is called the first critical angle. Take the incidence via organic acoustic wedge to a planar steel sheet for example. The first critical angle can be calculated by:

$$\theta_{\mathrm{L_{CR}}} = \arcsin(V_1/V_2) \quad (21)$$

where, V_1 and V_2 are the longitudinal wave speeds in the acoustic wedge and the steel plate, respectively.

For a curved member, the first critical angle $\theta_{\mathrm{L_{CR}}}$ satisfies:

$$\theta_{\mathrm{L_{CR}}} = \arcsin(\frac{V_1}{V_2}) \pm \frac{90L}{\pi R} \quad (22)$$

where, L is the propagation distance; R is the radius of curvature of the curved member, which is + for convex surfaces, and – for concave surfaces.

When the ultrasonic longitudinal wave is incident in the measured material at the first critical angle, critically refracted transverse wave and surface wave will be generated at the interface, in addition to the L_{CR} wave. With stress $\sigma = 0$ the elastic coefficient of steel in Tab. 1 was substituted to Eqs. (7) and (8) respectively to obtain the speeds of critically refracted horizontal and transverse waves $V_{\mathrm{L_{CR}}} = 5.96$ km/s and $V_{\mathrm{T_{CR}}} = 3.23$ km/s. When the Poisson's ratio $\nu = 0.3$, the surface wave speed $V_{\mathrm{R}} \approx 0.93V_{\mathrm{T_{CR}}} = 3.00$ km/s. Thus, L_{CR} wave is the fastest propagating wave.

4 CONSTRUCTION OF ULTRASONIC DETECTION SYSTEM

4.1 Excitation and Detection Depth of L_{CR} Wave

The L_{CR} wave was excited by pitch-catch oblique incidence within a certain depth of the measured material (Fig. 4).

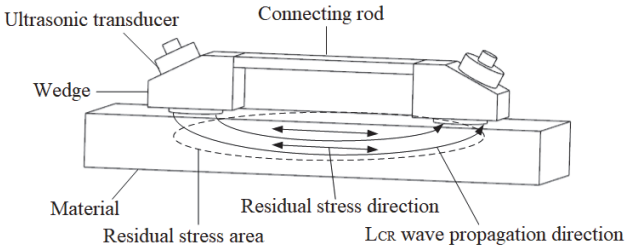

Figure 4 L_{CR} wave excitation device

When the L_{CR} wave propagates in the measured member with a finite thickness, the penetration depth is a function of frequency (wavelength). In general, the penetration depth of the L_{CR} wave is equal to one wavelength and a half [10]. Any change of frequency will change the detection depth. Hence, the horizontal stress distribution can be calculated for each particular depth, making it possible to evaluate the residual stress gradient based on the L_{CR} wave. However, the L_{CR} wave usually has a very low frequency. It is easy to excite a guide wave in a thin member, reducing the sensitivity to stress [11]. If the frequency is too high, the penetration depth would be too shallow; then, the test results will be greatly affected by surface roughness, and the waveform would attenuate significantly. Through comprehensive consideration, the center frequency was selected as 5 MHz [12].

4.2 Design of Curved Wedge

During the residual stress detection of tubular and shaft members (inner walls, air supply pipes, torque shafts, etc.), it is necessary to consider the effects of the component curvature on the excitation and propagation of the L_{CR} wave. This paper designs a curved acoustic wedge (Fig. 5).

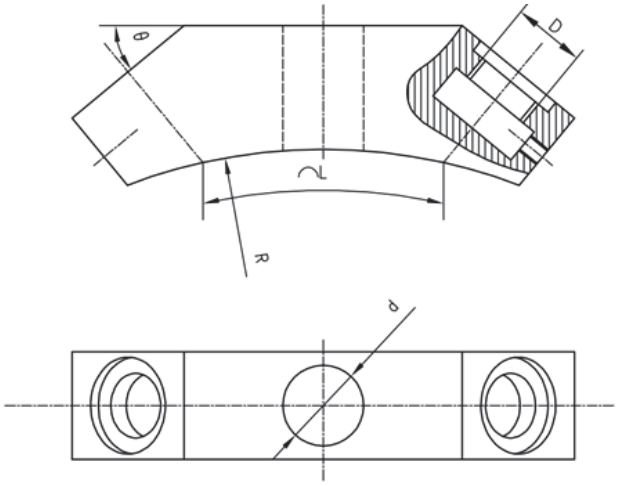

Figure 5 Curved wedge for residual stress detection

The propagation distance is denoted as L. To unify the signal strength and the stress resolution, the L value is generally set to 30 to 50 mm. The transducer radius and the radius of curvature of the member are denoted by D and R, respectively. The diameter of the through hole at the middle of the wedge is denoted as d, which prevents the ultrasonic wave from propagating from the sender to the receiver directly through the wedge. If the member is a ferromagnetic material, a magnetic absorption device can be mounted at the through hole. The incident angle for exciting the L_{CR} wave is denoted as θ, which can be calculated by Eq. (22).

4.3 Propagation Time Difference Algorithm

Our system densifies the collected data points through interpolation, and eliminates the influence of coupling layer thickness and bottom echo through system delay, stability criterion, and cross-correlation calculation. The theoretical precision of residual stress detection thus reached ±10 MPa.

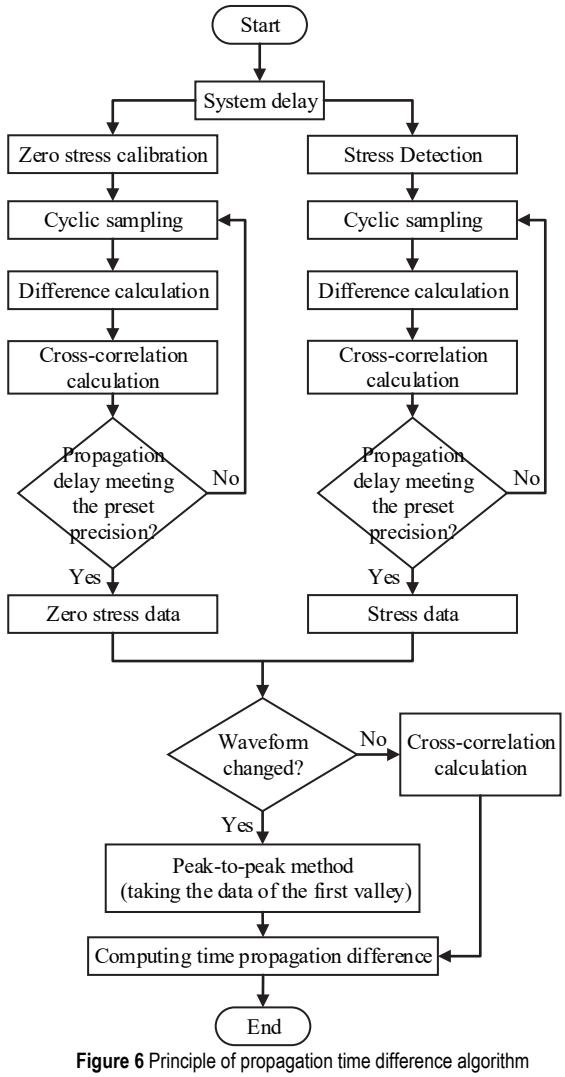

Figure 6 Principle of propagation time difference algorithm

Fig. 6 explains the principle of our propagation time difference algorithm.

5 EXPERIMENTAL ANALYSIS

Our experiments target a 4m-long segment of S685 steel barrel with the diameter of 105 mm. Eight normal

were selected along the directions of 0°, 45°, 90°, 135°, 180°, 225°, 270°, and 315°.

(a) Automatic crawling mechanism

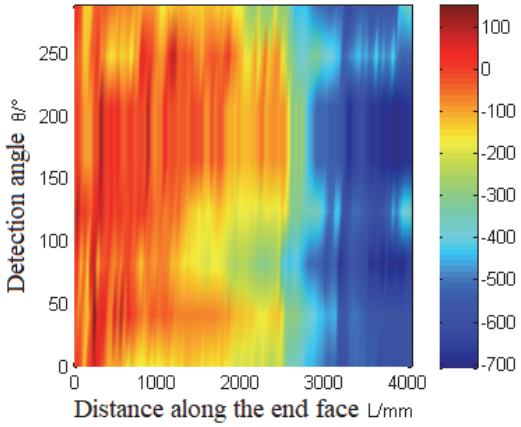

(b) Cloud map of inner wall stress distribution

Figure 7 Ultrasonic nondestructive detection of self-compacting stress of barrel

Along each normal, the automatic crawling mechanism (Fig. 7a) moved at a step length of 40 mm, and made one detection in each step. As shown in Fig. 7b, the detection results agree with the stress field distribution obtained by the destructive slice method; the whole process takes just 40 minutes. Therefore, our ultrasonic detection method is accurate and fast.

6 CONCLUSIONS

(1) The principle of ultrasonic detection of residual stress was analyzed based on acoustic elasticity theory. After comparing the stress sensitivity coefficients of different types of waves, it is concluded that the longitudinal wave propagating along the stress direction is the most sensitive to stress.

(2) According to Snell's law, the L_{CR} wave can be generated using the first critical angle. This wave can propagate far through the material, and achieve a faster speed than other waves. Besides, the L_{CR} wave propagating along the stress direction is the most sensitive to stress. These properties facilitate signal processing.

(3) The distribution law of the mean stress at each particular depth can be calculated by changing the main frequencies of the excitation and receiving probes with a fixed interval. This could help the evaluation of residual stress gradient.

(4) This paper designs a curved wedge for detecting the residual stress of tubular members. In terms of software, system delay, stability criterion, and cross-correlation calculation were adopted to increase the theoretical precision of residual stress detection to ±10 MPa.

(5) The ultrasonic stress detection technique was applied to detect the self-compacting stress field of barrel inner wall. The cloud map of the stress field was obtained quickly and accurately, solving the difficult issue of detecting the self-compacting stress on inner walls.

Acknowledgements

This work is funded by Natural Science Foundation of Hebei Province (E2019210309, E2019210299), and Science and Technology Research Project of Higher Education in Hebei Province (QN2018016).

7 REFERENCES

[1] Totten, G. E., Howes, M., & Inoue, T. (2002). *Handbook of residual stress and deformation of steel*. New York, ASM International Publishers.

[2] Liu, C. & Zhuang, D. (2012). Internal welding residual stress measurement based on contour method. *Chinese Journal of Mechanical Engineering*, *48*(8), 54-59.

[3] Rossini, N. S., Dassisti, M., & Benyounis, K. Y., (2012). Methods of measuring residual stresses in components. *Materials and Design*, *35*, 572-588. https://doi.org/10.1016/j.matdes.2011.08.022

[4] Tatsuo, T. & Yukio, I. (1968). Acoustical birefringence of ultrasonic waves in deformed isotropic elastic materials. *International Journal Solids Structures*, *4*, 383-389. https://doi.org/10.1016/0020-7683(68)90045-0

[5] Hughes, D. S. & Kelly, J. L. (1953). Second-order elastic deformation of solids. *Physics Review*, *92*(5), 1145-1149. https://doi.org/10.1103/PhysRev.92.1145

[6] Pao, Y. H. & Sachse, W. (1984). Acoustoelasticity and ultrasonic measurement of residual stresses. *Physical Acoustics*, *17*, 62-140.

[7] Rose, J. L. (1999). *Ultrasonic waves in solid media.* Cambridge, Cambridge University Press.

[8] Duquennoy, M., Ouaftouh, M., & Qurak, M. (1999). Ultrasonic evaluation of stress in orthotropic materials using rayleigh waves. *NDT&E International*, *32*, 189-199. https://doi.org/10.1016/S0963-8695(98)00046-2

[9] Viktor, H. (1997). *Structural and residual stress analysis by nondestructive methods*. Netherlands, Elsevier Press.

[10] Chaki, S., Ke, W., & Demouveau, H. (2013). Numerical and experimental analysis of the critically refracted longitudinal beam. *Ultrasonics*, *53*, 65-69.

[11] Sadeghi, S., Najafabadi, M. A., & Javadi, Y. (2013). Using ultrasonic waves and finite element method to evaluate through-thickness residual stresses distribution in the friction stir welding of aluminum plates. *Materials and Design*, *52*, 870-880. https://doi.org/10.1016/j.matdes.2013.06.032

[12] Song, W. T., Xu, C. G., & Pan, Q. X. (2016). Nondestructive Testing and Characterization of Residual Stress Field Using an Ultrasonic Method. *Chinese Journal of Mechanical Engineering*, *29*(2), 365-371. https://doi.org/10.3901/CJME.2015.1023.126

Contact information:

Wentao SONG
School of Mechanical Engineering,
Shijiazhuang Tiedao University,
Shijiazhuang 050043, China
E-mail: 18810328150@163.com

Zengxu ZHAO
(Corresponding author)
School of Mechanical Engineering,
Shijiazhuang Tiedao University,
Shijiazhuang 050043, China
E-mail: songwt@stdu.edu.cn